



Development of a cavity enhanced aerosol albedometer

W. Zhao et al.

This discussion paper is/has been under review for the journal Atmospheric Measurement Techniques (AMT). Please refer to the corresponding final paper in AMT if available.

Development of a cavity enhanced aerosol albedometer

W. Zhao^{1,2}, X. Xu^{1,2}, M. Dong^{1,2}, W. Chen³, X. Gu^{1,2}, C. Hu^{1,2}, Y. Huang¹, X. Gao^{1,2}, W. Huang^{1,2}, and W. Zhang^{1,2}

¹Key Laboratory of Atmospheric Composition and Optical Radiation, Anhui Institute of Optics and Fine Mechanics, Chinese Academy of Sciences, Hefei 230031, Anhui, China

²Laboratory of Atmospheric Physico-Chemistry, Anhui Institute of Optics and Fine Mechanics, Chinese Academy of Sciences, Hefei 230031, Anhui, China

³Laboratory of Physical-Chemistry of the Atmosphere, University of the Littoral Opal Coast, 59140 Dunkerque, France

Received: 11 February 2014 – Accepted: 17 March 2014 – Published: 26 March 2014

Correspondence to: W. Zhang (wjzhang@aiofm.ac.cn)

Published by Copernicus Publications on behalf of the European Geosciences Union.

Title Page

Abstract

Introduction

Conclusions

References

Tables

Figures



Back

Close

Full Screen / Esc

Printer-friendly Version

Interactive Discussion



Abstract

We report on the development of a cavity enhanced aerosol single scattering albedometer incorporating incoherent broad-band cavity-enhanced spectroscopy (IB-BCEAS) approach and an integrating sphere (IS) for simultaneous in situ measurements of aerosol scattering and extinction coefficients in the exact same sample volume. The cavity enhanced albedometer employed a blue light-emitting diode (LED) based IBBCEAS approach for the measurement of wavelength-resolved aerosol optical extinction over the spectral range of 445–480 nm. An integrating sphere nephelometer coupled to the IBBCEAS setup was used for the measurement of aerosol scattering. The scattering signal was measured with a single channel photomultiplier tube (PMT), providing an integrated value over a narrow bandwidth (FWHM \sim 9 nm) in the spectral region of 465–474 nm. A scattering coefficient at a wavelength of 470 nm was deduced as an averaged scattering value and used for data analysis and instrumental performance comparison. Performance evaluation of the albedometer was carried out using laboratory-generated particles and ambient aerosol. The scattering and extinction measurements of monodisperse polystyrene latex (PSL) spheres generated in laboratory proved excellent correlation between two channels of the albedometer. The retrieved refractive index (RI) from the measured scattering and extinction efficiencies agreed well with the values reported in previously published papers. Aerosol light scattering and extinction coefficients, single scattering albedo (SSA) and NO₂ concentrations in an ambient sample were directly and simultaneously measured using the developed albedometer. The developed instrument was validated via an intercomparison of the measured aerosol scattering coefficient and NO₂ trace concentration against a TSI 3563 integrating nephelometer and a chemiluminescence detector, respectively.

Development of a cavity enhanced aerosol albedometer

W. Zhao et al.

Title Page

Abstract

Introduction

Conclusions

References

Tables

Figures



Back

Close

Full Screen / Esc

Printer-friendly Version

Interactive Discussion



1 Introduction

Aerosol single scattering albedo (SSA, ω), defined as the ratio of the aerosol scattering (α_{scat}) to its extinction (α_{ext}) coefficient, is an important parameter that governs the relative strength of the aerosol scattering and absorption capacity. The value of SSA ranges from 0 for a completely absorbing particle to 1 for a purely scattering particle (Ramanathan et al., 2001; Chin et al., 2009; Hallquist et al., 2009). The in situ accurate measurement of SSA is a key challenge in atmospheric science and climate change research (Moosmüller et al., 2009; Yu et al., 2012; Petzold et al., 2013).

Since aerosol extinction coefficient is the sum of absorption and scattering coefficients, the commonly used method for the measurement of SSA is to separately measure the aerosol scattering, absorption and extinction coefficients with different instruments. In general, the aerosol absorption coefficient is measured with filter-based techniques, or photoacoustic spectroscopy (PAS) technique (Sheridan et al., 2005; Slowik et al., 2007; Cross et al., 2010; Lack et al., 2014). The scattering coefficient is usually measured with an integrating nephelometer and the extinction coefficient can be measured with an optical extinction cell or cavity-enhanced/ring-down spectroscopy (Moosmüller et al., 2009). Improving the detection sensitivity and the measurement accuracy for each optical parameter is of the first importance to improve the measurement accuracy of SSA.

The filter-based techniques, such as particle soot absorption photometer (PSAP), aethalometer and multi-angle absorption photometer (MAAP), are simple, low cost and insensitive to gaseous absorption. These techniques suffer, however, from the fact that the natural suspended state of the aerosol changed after deposition (Subramanian et al., 2007). The measurements are strongly influenced by filter type, multiple scattering by filter medium, and angular distribution of scattered light (Moosmüller et al., 2009). The measurement uncertainties of the filter-based techniques are typically between 20–30 % for laboratory generated dry non-absorbing or strong absorbing particles (Bond et al., 1999). For high relative humidity (RH) or highly light absorbing organic

Development of a cavity enhanced aerosol albedometer

W. Zhao et al.

Title Page

Abstract

Introduction

Conclusions

References

Tables

Figures



Back

Close

Full Screen / Esc

Printer-friendly Version

Interactive Discussion



**Development of
a cavity enhanced
aerosol albedometer**

W. Zhao et al.

Title Page

Abstract

Introduction

Conclusions

References

Tables

Figures



Back

Close

Full Screen / Esc

Printer-friendly Version

Interactive Discussion



aerosol plumes in the ambient atmosphere (Schneider et al., 2003; Virkkula et al., 2005; Chartier et al., 2012). Cavity-enhanced/ring-down spectroscopy provides a high sensitive and accurate method for α_{ext} measurement. The detection sensitivity can be better than 1 Mm^{-1} with an accuracy of $< 3\%$ (Sapcey et al., 1998; Smith and Atkinson, 2001; Thompson et al., 2002; Brown, 2003; Pettersson et al., 2004; Moosmüller et al., 2005; Kebabian et al., 2007; Abo Riziq et al., 2007; Zhang et al., 2008; Lang-Yona et al., 2009; Massoli et al., 2010; Li et al., 2011; Mellon et al., 2011; Bluvshstein et al., 2012; Michel Flores et al., 2012; Wang et al., 2012).

Combination of cavity-enhanced/ring-down method and photoacoustic technique has been used for high sensitive measurement of aerosol single scattering albedo without changing the dispersed state of the aerosol particles (Langridge et al., 2011; Lack et al., 2012). However, as this method involves still different instruments for separate measurements of extinction and absorption coefficients under different sampling conditions, it might cause potential errors in the determination of SSA value, because aerosol optical properties are very sensitive to the sampling conditions such as temperature and RH (Lack et al., 2008).

Various spectroscopic approaches have been developed for simultaneous measurement of aerosol scattering and extinction coefficients on the exact same sample volume to overcome this weakness, such as the recently developed Integrated Photoacoustic Nephelometer (Abu-Rahmah et al., 2006; Chakrabarty et al., 2007; Lewis et al., 2008; Chakrabarty et al., 2010; Sharma et al., 2013) and Cavity Ring-Down Nephelometer (Strawa et al., 2003, 2006; Sanford et al., 2008). A fixed frequency aerosol albedometer incorporating cavity ring-down spectroscopy and an integrating sphere for simultaneous measurement of optical scattering and extinction at a fixed frequency was developed by Thompson et al. (2008; Dial et al., 2012; Ma and Thompson, 2012; Wei et al., 2013a, b; Ma et al., 2013). The relative uncertainty in SSA achieved by this device, dependent upon the particle loading, is better than 5% (with detection sensitivities of 2.7 Mm^{-1} and 0.6 Mm^{-1} for scattering and extinction, respectively), which holds promise for the sensitive measurement of SSA.

resulting in a spectral resolution of 0.4 nm over the wavelength range of 412–487 nm. Temperature and relative humidity were measured with a hygrometer humidity sensor (Rotronic, model HC2).

The integrating sphere, machined from solid aluminum, was segmented into two hemispheres with an inner diameter d_0 of 15 cm. The inside layer of the IS consisted of pressed PTFE (with a uniform reflectivity of > 99 % between 200–2500 nm). The internal volume of the sphere was about 1.8 L. A 16 mm diameter hole was presented at each pole of the hemisphere for the passage of the probe light beam. A third hole of identical size was located on the side wall of one hemisphere, and was used for the scattering signal measurement with a photomultiplier tube (PMT, ZOLIX PMTH-S1-CR131A). A 2 cm wide light baffle, made of PTFE, was used to prevent light scattered by the medium from directly reaching the PMT. A bandpass filter, which centered at 470 nm with an FWHM of ~ 9 nm (470 nm_{-5}^{+4}), was located in the front of the PMT to eliminate the ambient stray light. The PMT signal was acquired with a DAQ card (National Instruments, NI PCIe-6351), which provided an integrated scattering signal over the spectral region of 465–474 nm.

3 Results and discussion

3.1 Angular nonidealities of the albedometer

The forward scattering truncation geometry of the developed cavity enhanced albedometer and a plot of truncation angles as a function of the distance d_e from the scattering location in the sphere to the exit or entrance aperture are shown in Fig. 2. Following Varma et al.'s (2003) discussion, the forward scattering truncation angle of our albedometer varied from 3.1° to 90° with an average of 12.2° for the integrating sphere without truncation reduction tube. The effective truncation angle $\alpha(d_e) = \tan^{-1}[r/(d_e + d_0)]$ varied from 1.2° to 3.1° (d_e and d_0 are schematized in

Development of a cavity enhanced aerosol albedometer

W. Zhao et al.

Title Page

Abstract

Introduction

Conclusions

References

Tables

Figures

◀

▶

◀

▶

Back

Close

Full Screen / Esc

Printer-friendly Version

Interactive Discussion



the figure and $r = 8$ mm), with an average value of 1.8° for particles located in the truncation-reduction tube at a distance d_e from the entrance aperture.

Figure 3 shows size dependent truncated fraction of total scattering for various truncation angles (Baynard et al., 2007). Four different truncation angles were calculated with different d_e representing different geometries: (1) $0-1.22^\circ$, with $d_e = (d - d_0)/2$, where d is the distance between two cavity mirrors; (2) $0-1.48^\circ$, $d_e = (L - d_0)/2$, with L the distance from the sample inlet to the outlet. (3) $0-3.1^\circ$, for the integrating sphere without truncation reduction tubes, and (4) $0-7^\circ$, in the case of TSI 3563 nephelometer (as specified by the manufacturer). The truncated fraction of total scattering was calculated with Mie scattering theory for spherical monodisperse particles with a RI of $m = 1.6 + i0$ at $\lambda = 470$ nm. For $1 \mu\text{m}$ diameter particle, truncated fractions of total scattering were 0.22 % and 1.4 % with (truncation angle of 1.22°) and without (truncation angle of 3.1°) truncation reduction tubes, respectively. The truncation-reduction tubes compensated for the near-forward scattered intensity, and reduced the measurement errors in large particle scattering measurements. This value of 0.22 % was much smaller than that from TSI nephelometer 6.4 %. The small truncation angle ($0-1.29^\circ$) of our IS system dramatically reduced truncation errors for large particles when compared with a TSI nephelometer.

3.2 Data retrieval processing

In IBBCEAS approach, wavelength resolved aerosol extinction can be calculated with the following equation (Fiedler et al., 2003; Washenfelder et al., 2008):

$$\begin{aligned}\alpha_{\text{Total Ext}}(\lambda) &= \alpha_{\text{Aerosol Ext}}(\lambda) + \alpha_{\text{Gas Abs}}(\lambda) \\ &= R_L \left(\frac{(1 - R(\lambda))}{d} + \alpha_{\text{Rayleigh}}(\lambda) \right) \left(\frac{I_0(\lambda) - I(\lambda)}{I(\lambda)} \right)\end{aligned}\quad (1)$$

where $R(\lambda)$ is the mirror reflectivity, d is the distance between two cavity mirrors, $I_0(\lambda)$ and $I(\lambda)$ are the light intensities transmitted through the cavity without and with air samples, respectively. In our experiment, $I_0(\lambda)$ is defined as a background spectrum of N_2

Development of a cavity enhanced aerosol albedometer

W. Zhao et al.

Title Page

Abstract

Introduction

Conclusions

References

Tables

Figures

◀

▶

◀

▶

Back

Close

Full Screen / Esc

Printer-friendly Version

Interactive Discussion



Development of a cavity enhanced aerosol albedometer

W. Zhao et al.

Title Page

Abstract

Introduction

Conclusions

References

Tables

Figures



Back

Close

Full Screen / Esc

Printer-friendly Version

Interactive Discussion



or zero air whose Rayleigh scattering coefficient $\alpha_{\text{Rayleigh}}(\lambda)$ is explicitly accounted. R_L is the ratio of the total cell length to the air sample cell length when the cavity mirror is purged with gas flow. The two components included in the measured total extinction $\alpha_{\text{Total Ext}}(\lambda)$: $\alpha_{\text{Aerosol Ext}}(\lambda)$ and $\alpha_{\text{Gas Abs}}(\lambda)$, correspond to the extinction coefficients related to aerosol extinction and gas phase absorption, respectively.

Broadband wavelength measurement of extinction coefficient by IBBCEAS provides a robust method for simultaneous and selective quantitative measurement of both aerosol extinction coefficient and multiple trace gas concentrations with a single instrument. The gas phase absorption can be extracted from the total extinction using the following equation:

$$\alpha_{\text{Total Ext}}(\lambda) = \sum n_i \sigma_i (s_i + t_i \lambda) + P(\lambda) \quad (2)$$

The first term describes the contribution of multiple gas absorptions and the 2nd includes the contribution from wavelength-dependent aerosol extinction. Where n_i and σ_i are the number density and the absolute absorption cross section of the i th absorber, respectively. s_i and t_i are the shift and stretch coefficients for each absorber, used to reconstruct an accurate wavelength calibration. The polynomial offset $P(\lambda)$, varying from linear to fifth order, is used to account for variation in spectral background including wavelength-dependent aerosol extinction and spectral baseline shift (which can be considered as system drift in the extinction measurement). In the present work, 3rd order polynomial function was used for data retrieval. For a particle-free sample, $P(\lambda)$ merely represents the spectral baseline drift including baseline variation due to Rayleigh scattering by air and unspecified background change in spectra resulting from unstable LED emission or/and unstable dark current variation in the CCD spectrometer. For this reason, high intensity stability of a IBBCEAS instrument is highly required for high-accuracy measurements of aerosol extinction such that the background drift could be negligible in comparison with the measured aerosol extinction (Zhao et al., 2013).

Development of a cavity enhanced aerosol albedometer

W. Zhao et al.

Title Page

Abstract

Introduction

Conclusions

References

Tables

Figures

◀

▶

◀

▶

Back

Close

Full Screen / Esc

Printer-friendly Version

Interactive Discussion



Mirror reflectivity $R(\lambda)$ of the albedometer was determined by introducing gases with different Rayleigh cross-section (Washenfelter et al., 2008; Zhao et al., 2013; Dong et al., 2013). In this work, the $R(\lambda)$ was determined from the difference in the transmitted intensities of N_2 and SF_6 . The cavity was flushed with N_2 and SF_6 at 1.5 L min^{-1} rate for 40 min for each species, until the transmitted light intensity attained a stable value. The Rayleigh cross sections used for the mirror reflectivity calculation were reported by Naus and Ubachs (2000) and Snee and Ubachs (2005), with an experimental uncertainty in cross section of 1 % for N_2 and 3 % for SF_6 . The mirror reflectivity was found to be about 99.96 % at 470 nm. During the process of mirror reflectivity calibration, the purging zero air flow was turned off and the cavity was fully filled with calibration gases. For aerosol measurement, zero air was continuously used which shortened the effective path length. R_L was determined from the absorption measurement of 42 ppbv NO_2 with and without mirror purges (Wu et al., 2009; Washenfelter et al., 2013).

The scattered light is proportional to the ratio of the scattering signal (I_{scat}) measured with a PMT and the transmitted intensity (I_{trans}) measured with a CCD spectrometer. When purging gas was continuously introduced in the albedometer, the effective path-length and thus the reduction tube length was shortened. However, for particle diameter smaller than $2 \mu\text{m}$, the truncation error was smaller than 2 %, and therefore the purging gas effect (R_L factor) might be neglected for the scattering measurement of our albedometer in this work (Strawa et al., 2003; Thompson et al., 2008):

$$\alpha_{\text{scat}} = \frac{I_{\text{scat}}}{I_{\text{trans}}} \frac{(1-R)}{(1+R)d} K = \frac{I_{\text{scat}}}{I_{\text{trans}}} K' \quad (3)$$

where K and K' are the experimentally determined calibration constants that account for the differences in collection efficiency and response of different type of detectors, respectively. The calibration of the parameter K' can be made based on the assumption of a linear response of the PMT signal to scattering light intensity (Anderson et al., 1996). K' might be simply calibrated with CO_2 and N_2 scattering processes by the

following equation:

$$K' = (\alpha_{\text{scat_CO}_2} - \alpha_{\text{scat_N}_2}) / \left(\frac{I_{\text{scat_CO}_2}}{I_{\text{trans_CO}_2}} - \frac{I_{\text{scat_N}_2}}{I_{\text{trans_N}_2}} \right) \quad (4)$$

where $\alpha_{\text{scat_CO}_2}$ and $\alpha_{\text{scat_N}_2}$ are the theoretically calculated Rayleigh scattering coefficients of CO₂ and N₂. $I_{\text{scat_CO}_2}$ and $I_{\text{scat_N}_2}$ are experimentally measured scattering intensities when the cavity is filled with CO₂ or N₂, respectively. $I_{\text{trans_CO}_2}$ and $I_{\text{trans_N}_2}$ are the measured transmitted intensity (at $\lambda = 470$ nm in our case) for CO₂ and N₂, respectively.

In order to well calibrate the scale factor K' , He and SF₆ were used to extend the dynamical range (from 0.3 to 145 Mm⁻¹) of the calibration. The Rayleigh scattering cross section for He was fitted to Shardanand and Rao's data ($\sigma_{\text{Rayleigh He}} = 1.336 \times 10^{-17} \times \lambda^{-4.1287}$) (Shardanand and Rao, 1977; Washenfelder et al., 2013). The cross sections of N₂, CO₂, and SF₆ were obtained from Naus and Ubachs (2000), and Sneep and Ubachs (2005). Calibration of K' was achieved by flushing the cavity with calibration gases and then performing measurements of the $I_{\text{scat}}/I_{\text{trans}}$ ratio. A linear fit of the theoretical value of the Rayleigh scattering coefficient of each gas to the measured $I_{\text{scat}}/I_{\text{trans}}$ is shown in Fig. 4a. As can be seen, the measured $I_{\text{scat}}/I_{\text{trans}}$ signal is linearly correlated with the theoretically calculated Rayleigh scattering coefficient. The intercept of the $I_{\text{scat}}/I_{\text{trans}}$ ratio was considered as the contribution of the photon counts due to scattering by internal surfaces.

A regression plot of the measured extinction and scattering coefficients for calibration gases is shown in Fig. 4b, which proves an excellent correlation between the scattering and the extinction measurements (Scattering = $-0.288 (\pm 0.869) + 0.998 (\pm 0.018) \times$ Extinction, with $R^2 = 0.9987$).

Development of a cavity enhanced aerosol albedometer

W. Zhao et al.

Title Page

Abstract

Introduction

Conclusions

References

Tables

Figures

◀

▶

◀

▶

Back

Close

Full Screen / Esc

Printer-friendly Version

Interactive Discussion



3.3 Precision and accuracy of the instrument

The detection limits for the measurement of the scattering and extinction coefficients at 470 nm were determined by an Allan variance analysis. Figure 5 shows an Allan deviation plot realized based on 5.5 h time series measurements of a particle free zero air sample with a time resolution of 9 s. Longer-term drift of the instrument was observed and smaller than 2 Mm^{-1} . The scattering measurement channel exhibited the lowest detection limit of 0.07 Mm^{-1} with an optimum integration time of 459 s that was much longer than the optimum integration time for the extinction measurement channel (54 s). With 54 s integration time, the detection limits for the scattering and extinction channels were 0.22 Mm^{-1} and 0.09 Mm^{-1} , respectively.

In the lower panel of Fig. 5, frequency distributions of the scattering and extinction measurements are shown. A Gaussian distribution was fitted to the histograms to obtain the mean of the zero air measurements and the standard deviation (Kennedy et al., 2011; Dorn et al., 2013). The 1σ standard deviation of the Gaussian fit is a measure of the actual instrument precision. The determined extinction measurement precision of 0.51 Mm^{-1} (in 9 s) is comparable to the result reported by Petzold et al. (0.19 Mm^{-1} with 10 s average time) (Petzold et al., 2013).

For aerosol measurement, the accuracy in the extinction measurement is mainly limited by the uncertainties in $(1 - R)$, R_L and particle losses in the cavity. The drift of the LED intensity is not included, since frequent recording of I_0 could allow correction for the baseline drift related to the fluctuation in LED emission intensity. The mean uncertainty in the determined $(1 - R)$ was less than 1%. We estimated an uncertainty of 3% in R_L . The particle loss through the system, determined via the measurements from two condensation particle counters installed at the inlet and the outlet respectively, was estimated to be 2%. Considering all of the uncertainties, the total uncertainty in the extinction measurement was estimated to be less than 5%.

The uncertainty in the scattering measurement is mainly caused by the uncertainties in K' , the error caused by the angular nonidealities (less than 2% for particle diameter

Development of a cavity enhanced aerosol albedometer

W. Zhao et al.

Title Page

Abstract

Introduction

Conclusions

References

Tables

Figures



Back

Close

Full Screen / Esc

Printer-friendly Version

Interactive Discussion



smaller than 2 μm), and particle loss in the cavity. The uncertainty of K' was less than 2%. The total uncertainty in scattering measurement was estimated to be about 4%.

The total uncertainty of SSA was then estimated to be less than 5%. Where the $(1 - R)$ and R_L errors were considered as the total extinction error, while the errors in K' , and angular nonidealities were considered as the total scattering error. Since the scattering and extinction coefficients were measured on the exact same volume, the uncertainty due to particle losses could be ignored. However, for particle diameters larger than 2 μm , the influence of truncation errors and near-forward scattering corrections for the finite acceptance angle extinction measurements may be potential error sources.

3.4 Instrument test using laboratory generated particles

Performance evaluation of the developed albedometer was performed with measurements of laboratory generated monodispersed polystyrene latex (PSL) spheres. The aerosol generation system was the same as used in our previously work (Zhao et al., 2013). Aerosols were generated with a constant output atomizer (TSI-3076). A monodisperse distribution was generated by an electrostatic classifier (TSI differential mobility analyzer, DMA 3080 L). PSL standards of four different diameters (200, 240, 300 and 400 nm) were generated and used for the evaluation. The particle concentration was determined with two condensation particle counters (a CPC 3775 at the entrance of the cavity and a CPC 3776 at the exit of the cavity). The averaged particle number, after taking into account the dilution inside the cavity as a result of the purge flow of zero air on the mirrors, was used for data analysis.

Figure 6a shows a regression plot of the extinction and scattering coefficients ($\alpha_{\text{scat, ext}}$) at $\lambda = 470 \text{ nm}$. The scattering and extinction data were averaged over 5 to 10 min sequences after the aerosol number concentration in the cell was sufficiently stable. Error bars in the figure correspond to 1σ of the sequence average. For the measurements of different PSL number concentrations or diameters, the cavity was washed with zero air for acquisition of $I_0(\lambda)$ spectrum in order to correct for drifts in the background spectrum. The transmitted and scattered intensities of the particle free

Development of a cavity enhanced aerosol albedometer

W. Zhao et al.

Title Page

Abstract

Introduction

Conclusions

References

Tables

Figures

◀

▶

◀

▶

Back

Close

Full Screen / Esc

Printer-friendly Version

Interactive Discussion



sample were used to subtract the light scattered by internal surfaces and by gas portion of the sample. The non-absorbing PSL sphere experiments proved excellent correlation between the scattering and extinction measurements of the albedometer.

Plot of the experimentally measured scattering and extinction coefficients vs. the averaged value of the measured particle number concentration (N) is shown in Fig. 6b. The optical cross section ($\sigma_{\text{scat, ext}} = \alpha_{\text{scat, ext}}/N$) for each particle size was obtained by averaging the measurements at different concentrations. The scattering and extinction efficiencies ($Q_{\text{Scat, Ext}} = 4\sigma_{\text{Scat, Ext}}/\pi D^2$) were obtained as the ratio of the particle cross section to the geometric cross section. A plot of experimental $Q_{\text{Scat, Ext}}$ as a function of particle diameter is shown in Fig. 6c. The retrieval algorithm of the RI was realized by fitting the measured scattering and extinction efficiencies to theoretically calculated values based on Mie scattering subroutine, reported by Bohren and Huffman for homogeneous spheres (Bohren and Huffman, 1983; Laven, 2006). Best fit results were obtained by varying the real and imaginary parts of the RI. A set of RI was found by minimizing the “merit function” $\chi^2 \text{Num}^{-2}$, where χ^2 is (Dinar et al., 2008; Zarzana et al., 2012):

$$\chi^2(n, k) = \sum_{i=1}^{\text{Num}} \frac{(Q_{\text{scat, ext_measured}} - Q_{\text{scat, ext}}(n, k))_i^2}{\Delta Q_i^2} \quad (5)$$

where Num is the number of measurements (of different particle sizes) used in the fit, and ΔQ is the standard deviation of each measurement of the same particle size but at different concentrations.

The merit function was calculated for a wide range of n and k values, and the value of n and k that gives the lowest χ^2 (χ_0^2) was taken to be the retrieved RI. The values of n and k that satisfy $\chi^2 < \chi_0^2 + 2.298$ are considered within 1σ error bound of the best measurement (with 68.3% confidence level of χ^2 distribution). Projections of the contour lines (with a contour value of 2.298) on the n and k plane give the standard error Δn and Δk , respectively.

Development of a cavity enhanced aerosol albedometer

W. Zhao et al.

Title Page

Abstract

Introduction

Conclusions

References

Tables

Figures

◀

▶

◀

▶

Back

Close

Full Screen / Esc

Printer-friendly Version

Interactive Discussion



Development of a cavity enhanced aerosol albedometer

W. Zhao et al.

Title Page

Abstract

Introduction

Conclusions

References

Tables

Figures

◀

▶

◀

▶

Back

Close

Full Screen / Esc

Printer-friendly Version

Interactive Discussion



The RI of PSL was retrieved with scattering and extinction efficiencies, independently. The retrieved RI was $m = 1.676_{-0.008}^{+0.009} + i0.015_{-0.008}^{+0.009}$ from the scattering channel and $m = 1.674_{-0.012}^{+0.012} + i0_{0}^{+0.003}$ from the extinction channel, respectively. Limited by our aerosol generation system, the particles number concentrations were very small for the particle diameters larger than 400 nm. By using the efficiencies measured with small particle diameters for the fit of the merit function, a non-zero value of the imaginary part of RI could not be ruled out

Our results were agree with the literature reported RI values. Washenfelder et al. (2013) reported a value of $m = 1.633 + i0.005$ at $\lambda = 420$ nm. Chartier and Greenslade (2012) reported a value of $m = 1.72 + i0.005$ for PSL aerosol at $\lambda = 355$ nm, and Abo Rizip et al. (2007) and Bluvshstein et al. (2012) reported a value of $m = 1.597 + i0.005$ from cavity ring down-based aerosol extinction measurements at $\lambda = 532$ nm. Our results were also in close agreement with the RI value given by Nikolov and Ivanov (2000). At $\lambda = 470$ nm, interpolation of their data gave $m = 1.607 + i0$. The difference between our retrieved refractive index and this interpolation value was about 4 %, within the tolerance of the instrumental accuracy (4 % for scattering, 5 % for extinction coefficient measurements and 3 % for particle concentration measurement), which confirms that the original gas phase-based calibration of the mirror reflectivity $R(\lambda)$, scattering parameter K' , and R_L was suitable for the aerosol optical properties measurement.

3.5 Ambient measurement

For further evaluation and validation of the developed instrument, field environment measurements were carried out outside the laboratory at Anhui Institute of Optics and Fine Mechanics (31°54'18" N, 117°9'42" E) during the period of 18–19 April 2013. Ambient air was sampled through a copper pipe (22 mm inner diameter) with an inlet about 5 m above the ground level. The acquisition time of the albedometer for each data was 9 s (for 1.5 s integrating time per spectrum, and six spectra averaging). The cavity was

flushed with dry zero air every one hour for acquisition of $I_0(\lambda)$ spectrum. The transmitted and scattered intensities of the particle free (and non absorbing) air sample were used to subtract the light scattered by internal surfaces and by gas portion of the sample.

5 A representative of data retrieval is shown in Fig. 7 for ambient measurement at two different aerosol loadings: aerosol extinction larger than 400 Mm^{-1} (a, b), and lower than 100 Mm^{-1} (c, d) with different fit windows: full window of 444–481 nm for aerosol extinction determination (a, c), and narrow window of 444–467 nm for NO_2 concentration retrieval (b, d). The used NO_2 cross section reference was generated by convolution of high-resolution absorption cross sections reported by Vandaele et al. (2002) with the slit function of the spectrometer at 294 K. The H_2O absorption cross section was calculated based on the HITRAN 2008 database (Rothman et al., 2009). Large fit error observed around 475–481 nm was due to the relative low light transmitted intensity of the cavity. The detection sensitivity for ambient air measurements was lower than that obtained in particle free sample measurement: approximately 6 times lower for the aerosols with extinction larger than 400 Mm^{-1} and 3 times lower for the extinction smaller than 100 Mm^{-1} . Under higher aerosol loading condition, the detection sensitivity deteriorated and the NO_2 concentration retrieved from the full window (used for aerosol extinction determination) was a little larger than that from a narrow window (for NO_2 absorption retrieval).

15 An overview of ambient aerosol scattering, extinction coefficients, single scattering albedo (SSA) and NO_2 concentration measured by the developed albedometer is shown in Fig. 8. The particle number concentration and the relative humidity are also shown in the upper panel.

25 NO_2 concentrations retrieved from the IBBCEAS spectra were compared to the values measured with an online NO_x analyzer (Thermo 42i). Good agreement between two analytical instruments can be observed in Fig. 8b, except the period from 21:00 LT on 18 April to 06:00 LT on 19 April, where the results from the NO_x analyzer measurement were about 1.2 ppbv larger than the albedometer measurement results. This was

Development of a cavity enhanced aerosol albedometer

W. Zhao et al.

Title Page

Abstract

Introduction

Conclusions

References

Tables

Figures

◀

▶

◀

▶

Back

Close

Full Screen / Esc

Printer-friendly Version

Interactive Discussion



Development of a cavity enhanced aerosol albedometer

W. Zhao et al.

Title Page

Abstract

Introduction

Conclusions

References

Tables

Figures

◀

▶

◀

▶

Back

Close

Full Screen / Esc

Printer-friendly Version

Interactive Discussion



probably caused by the interference of NO_y measured by the NO_x analyzer (equipped with a molybdenum converter) (Villena et al., 2012). However, these differences were still around the tolerance of the NO_x detection sensitivity (1 ppbv). An enlarged drawing of the NO_2 measurement comparison in two selected periods (10:00–15:00 LT on 18 April for high aerosol load condition and 6:00–14:00 LT on 19 April for low aerosol loading) is shown in Fig. 9. NO_2 concentrations retrieved with different fit windows are also shown in the figure. From a correlation plot of the 5 min averaged data (Fig. 10), very good agreement was observed between two instruments for different aerosol loadings (Albedometer = $0.995 \times \text{NO}_x$ analyzer + 0.465 ppbv, with $R^2 = 0.956$).

The aerosol scattering coefficient measured by the developed cavity enhanced albedometer was compared with the data from an integrating nephelometer (TSI 3563) operating at three wavelengths centered at 453, 554 and 698 nm (the nominal values were 450, 550 and 700 nm, respectively) with a sample flow of 20 L min^{-1} . The data averaging time was 300 s. Zero adjusting was done automatically every one hour. The scattering coefficient at 470 nm from the TSI 3563 nephelometer was calculated based on the following equation (Massoli et al., 2009; Huang et al., 2012):

$$\alpha_{\text{scat}, 470} = \alpha_{\text{scat}, 453} \left(\frac{470}{453} \right)^{-\mathring{\text{a}}} \quad (6)$$

where the scattering Ångström exponent $\mathring{\text{a}} = -\frac{\log(\alpha_{\text{scat}, 453}/\alpha_{\text{scat}, 698})}{\log(453/698)}$ was calculated using the actual center wavelength values of 453 and 698 nm.

The scattering coefficients measured with the TSI 3563 agreed well with that from the albedometer, as shown in Fig. 8c. An enlarged drawing of the scattering and extinction measurements in this time interval is shown in Fig. 11a. Correlation of the scattering coefficients measured with two types of the instruments is plotted in Fig. 11b. Each data were five minutes averaged. Scattering coefficient measurements with the albedometer are highly correlated with those from the TSI 3563 (Albedometer = $1.13 \times \text{TSI Nephelometer} - 9.44 \text{ M m}^{-1}$, with $R^2 = 0.994$). The slope of 1.13 implicated that the smaller

truncation angle of the used integrating sphere in the cavity enhanced albedometer allowed for collection of more scattered light when compared to the TSI 3563 nephelometer. The intercomparison between the albedometer and the TSI nephelometer demonstrated the robustness of our instrument for ambient air measurement.

4 Conclusions

LED is a promising new type of light source, with long life time, low energy consumption and more compact than commonly used broadband arc lamps. High quality diode laser current and temperature controllers is usually used as LED controllers. In such way, high performance of the LED source is confidently achievable: very stable emission spectrum and optical output power, which allows for high sensitivity spectroscopic measurements of multi-species (aerosols and gases).

We report in this paper on the demonstration of a LED based cavity enhanced albedometer for simultaneous in situ measurement of aerosol scattering and extinction coefficients on the exact same sample volume. The performance of the instrument was evaluated using both laboratory generated particles and ambient aerosols. The cavity enhanced albedometer holds great promise for high sensitivity and high precision measurement of ambient aerosol scattering and extinction coefficients (hence SSA determination), and absorbing trace gas concentration.

At current stage, only one scattering coefficient can be measured due to the use of a single channel PMT. When replacing this single channel PMT with a multichannel PMT or a high sensitivity spectrometer, measurement of broadband wavelength resolved scattering coefficients could be achievable. Employing a multi-cavity configuration could allow the albedometer working in a wider wavelength range from the UV to the near IR.

Acknowledgements. This research is supported by the Instrument Developing Project of the Chinese Academy of Sciences (YZ201121), the National Basic Research Program of China (2013CB955802), the National Natural Science Foundation of China (No. 41005017,

Development of a cavity enhanced aerosol albedometer

W. Zhao et al.

Title Page

Abstract

Introduction

Conclusions

References

Tables

Figures

◀

▶

◀

▶

Back

Close

Full Screen / Esc

Printer-friendly Version

Interactive Discussion



41330424, 41375127) and the China Special Fund for Meteorological Research in the Public Interest (GYHY201406039). The support of the CaPPA project (“Chemical and Physical Properties of the Atmosphere”), funded by the French National Research Agency through the “Programme d’Investissement d’Avenir” (under contract ANR-10-LABX-005), is acknowledged.

We thank Professor Zhang Liming, Mr. Shen Zhengguo, and Mr. Qin Xiuhong in AIOFM for helpful discussions in the construction of the integrating sphere.

References

Abo Riziq, A., Erlick, C., Dinar, E., and Rudich, Y.: Optical properties of absorbing and non-absorbing aerosols retrieved by cavity ring down (CRD) spectroscopy, *Atmos. Chem. Phys.*, 7, 1523–1536, doi:10.5194/acp-7-1523-2007, 2007.

Abu-Rahmah, A., Arnott, W. P., and Moosmüller, H.: Integrating nephelometer with a low truncation angle and an extended calibration scheme, *Meas. Sci. Technol.*, 17, 1723–1732, 2006.

Anderson, T. L. and Ogren, J. A.: Determining aerosol radiative properties using the TSI 3563 integrating nephelometer, *Aerosol Sci. Tech.*, 29, 57–69, 1998.

Anderson, T. L., Covert, D. S., Marshall, S. F., Laucks, M. L., Charlson, R. J., Waggoner, A. P., Ogren, J. A., Caldow, R., Holm, R. L., Quant, F. R., Sem, G. J., Wiedensohler, A., Ahlquist, N. A., and Bates, T. S.: Performance characteristics of a high-sensitivity, three-wavelength, total scatter/backscatter nephelometer, *J. Atmos. Ocean. Technol.*, 13, 967–986, 1996.

Arnott, W. P., Moosmüller, H., Sheridan, P. J., Ogren, J. A., Raspert, R., Slaton, W. V., Hand, J. L., Kreidenweis, S. M., and Collett Jr., J. L.: Photoacoustic and filter-based ambient aerosol light absorption measurements: Instrument comparisons and the role of relative humidity, *J. Geophys. Res.*, 108, 4034, doi:10.1029/2002JD002165, 2003.

Baynard, T., Lovejoy, E. R., Pettersson, A., Brown, S. S., Lack, D., Osthoff, H., Massoli, P., Ciciora, S., Dube, W. P., and Ravishankara, A. R.: Design and application of a pulsed cavity ring-down aerosol extinction spectrometer for field measurements, *Aerosol Sci. Tech.*, 41, 447–462, 2007.

Bluvshstein, N., Flores, J. M., Abo Riziq, A., and Rudich, Y.: An approach for faster retrieval of aerosols’ complex refractive index using cavity ring-down spectroscopy, *Aerosol Sci. Tech.*, 46, 1140–1150, 2012.

Development of a cavity enhanced aerosol albedometer

W. Zhao et al.

Title Page

Abstract

Introduction

Conclusions

References

Tables

Figures

◀

▶

◀

▶

Back

Close

Full Screen / Esc

Printer-friendly Version

Interactive Discussion



Development of a cavity enhanced aerosol albedometer

W. Zhao et al.

Title Page

Abstract

Introduction

Conclusions

References

Tables

Figures

◀

▶

◀

▶

Back

Close

Full Screen / Esc

Printer-friendly Version

Interactive Discussion



- Bohren, C. F. and Huffman, D. R.: Absorption and Scattering of Light by Small Particles, Wiley, New York, 1983.
- Bond, T. C., Anderson, T. L., and Campbell, D.: Calibration and Intercomparison of Filter-Based Measurements of Visible Light Absorption by Aerosols, *Aerosol Sci. Tech.*, 30, 582–600, 1999.
- 5 Brown, S. S.: Absorption spectroscopy in high-finesse cavity for atmospheric studies, *Chem. Rev.*, 103, 5219–5238, 2003.
- Cappa, C. D., Lack, D. A., Burkholder, J. B., and Ravishankara, A. R.: Bias in filter-based aerosol light absorption measurements due to organic aerosol loading: evidence from laboratory
- 10 Measurements, *Aerosol Sci. Tech.*, 42, 1022–1032, 2008.
- Chakrabarty, R. K., Moosmüller, H., Arnott, W. P., Garro, M. A., Slowik, J. G., Cross, E. S., Han, J. H., Davidovits, P., Onasch, T. B., and Worsnop, D. R.: Light scattering and absorption by fractal-like carbonaceous chain aggregates: comparison of theories and experiment, *Appl. Optics*, 46, 6990–7006, 2007.
- 15 Chakrabarty, R. K., Moosmüller, H., Chen, L.-W. A., Lewis, K., Arnott, W. P., Mazzoleni, C., Dubey, M. K., Wold, C. E., Hao, W. M., and Kreidenweis, S. M.: Brown carbon in tar balls from smoldering biomass combustion, *Atmos. Chem. Phys.*, 10, 6363–6370, doi:10.5194/acp-10-6363-2010, 2010.
- Chartier, R. T. and Greenslade, M. E.: Initial investigation of the wavelength dependence of optical properties measured with a new multi-pass Aerosol Extinction Differential Optical Absorption Spectrometer (AE-DOAS), *Atmos. Meas. Tech.*, 5, 709–721, doi:10.5194/amt-5-709-2012, 2012.
- 20 Chin, M., Kahn, R. A., and Schwartz, S. E. (Eds.): Atmospheric Aerosol Properties and Climate Impacts, a Report by the US Climate Change Science Program and the Subcommittee on Global Change Research, National Aeronautics and Space Administration, Washington, DC, USA, 2009.
- 25 Cross, E. S., Onasch, T. B., Ahern, A., Wrobel, W., Slowik, J. G., Olfert, J., Lack, D. A., Massoli, P., Cappa, C. D., Schwarz, J. P., Spackman, J. R., Fahey, D. W., Sedlacek, A., Trimborn, A., Jayne, J. T., Freedman, A., Williams, L. R., Ng, N. L., Mazzoleni, C., Dubey, M., Brem, B., Kok, G., Subramanian, R., Freitag, S., Clarke, A., Thornhill, D., Marr, L. C., Kolb, C. E., Worsnop, D. R., and Davidovits, P.: Soot particle studies – instrument inter-comparison – project overview, *Aerosol Sci. Tech.*, 44, 592–611, 2010.
- 30

**Development of
a cavity enhanced
aerosol albedometer**

W. Zhao et al.

Title Page

Abstract

Introduction

Conclusions

References

Tables

Figures

◀

▶

◀

▶

Back

Close

Full Screen / Esc

Printer-friendly Version

Interactive Discussion



- Dial, K. D., Hiemstra, S., and Thompson, J. E.: Simultaneous measurement of optical scattering and extinction on dispersed aerosol samples, *Anal. Chem.*, 82, 7885–7896, 2012.
- Dinar, E., Abo Riziq, A., Spindler, C., Erlick, C., Kiss, G., and Rudich, Y.: The complex refractive index of atmospheric and model humic-like substances (HULIS) retrieved by a cavity ring down aerosol spectrometer (CRD-AS), *Faraday Discuss.*, 137, 279–295, 2008.
- 5 Dong, M., Zhao, W., Huang, M., Chen, W., Hu, C., Gu, X., Pei, S., Huang, W., and Zhang, W.: Near-ultraviolet incoherent broadband cavity enhanced absorption spectroscopy for OCIO and CH₂O in Cl-initiated photooxidation experiment, *Chin. J. Chem. Phys.*, 26, 133–139, 2013.
- 10 Dorn, H.-P., Apodaca, R. L., Ball, S. M., Brauers, T., Brown, S. S., Crowley, J. N., Dubé, W. P., Fuchs, H., Häsel, R., Heitmann, U., Jones, R. L., Kiendler-Scharr, A., Labazan, I., Langridge, J. M., Meinen, J., Mentel, T. F., Platt, U., Pöhler, D., Rohrer, F., Ruth, A. A., Schlosser, E., Schuster, G., Shillings, A. J. L., Simpson, W. R., Thieser, J., Tillmann, R., Varma, R., Venables, D. S., and Wahner, A.: Intercomparison of NO₃ radical detection instruments in the atmosphere simulation chamber SAPHIR, *Atmos. Meas. Tech.*, 6, 1111–1140, doi:10.5194/amt-6-1111-2013, 2013.
- 15 Fiedler, S. E., Hese, A., and Ruth, A. A.: Incoherent broad-band cavity-enhanced absorption spectroscopy, *Chem. Phys. Lett.*, 371, 284–294, 2003.
- Hallquist, M., Wenger, J. C., Baltensperger, U., Rudich, Y., Simpson, D., Claeys, M., Dommen, J., Donahue, N. M., George, C., Goldstein, A. H., Hamilton, J. F., Herrmann, H., Hoffmann, T., Iinuma, Y., Jang, M., Jenkin, M. E., Jimenez, J. L., Kiendler-Scharr, A., Maenhaut, W., McFiggans, G., Mentel, Th. F., Monod, A., Prévôt, A. S. H., Seinfeld, J. H., Surratt, J. D., Szmigielski, R., and Wildt, J.: The formation, properties and impact of secondary organic aerosol: current and emerging issues, *Atmos. Chem. Phys.*, 9, 5155–5236, doi:10.5194/acp-9-5155-2009, 2009.
- 20 Huang, Y., Li, L., Li, J., Wang, X., Chen, H., Chen, J., Yang, X., Gross, D. S., Wang, H., Qiao, L., and Chen, C.: A case study of the highly time-resolved evolution of aerosol chemical and optical properties in urban Shanghai, China, *Atmos. Chem. Phys.*, 13, 3931–3944, doi:10.5194/acp-13-3931-2013, 2013.
- 30 Kebabian, P. L., Robinson, W. A., and Freedman, A.: Optical extinction monitor using cw cavity enhanced detection, *Rev. Sci. Instrum.*, 78, 063102, doi:10.1063/1.2744223, 2007.
- Kennedy, O. J., Ouyang, B., Langridge, J. M., Daniels, M. J. S., Bauguitte, S., Freshwater, R., McLeod, M. W., Ironmonger, C., Sendall, J., Norris, O., Nightingale, R., Ball, S. M., and

**Development of
a cavity enhanced
aerosol albedometer**

W. Zhao et al.

Title Page

Abstract

Introduction

Conclusions

References

Tables

Figures

◀

▶

◀

▶

Back

Close

Full Screen / Esc

Printer-friendly Version

Interactive Discussion



Jones, R. L.: An aircraft based three channel broadband cavity enhanced absorption spectrometer for simultaneous measurements of NO_3 , N_2O_5 and NO_2 , *Atmos. Meas. Tech.*, 4, 1759–1776, doi:10.5194/amt-4-1759-2011, 2011.

Lack, D. A., Lovejoy, E. R., Baynard, T., Pettersson, A., and Ravishankara, A. R.: Aerosol absorption measurement using photoacoustic spectroscopy: sensitivity, calibration, and uncertainty developments, *Aerosol Sci. Tech.*, 40, 697–708, 2006.

Lack, D. A., Cappa, C. D., Covert, D. S., Baynard, T., Massoli, P., Sierau, B., Bates, T. S., Quinn, P. K., Lovejoy, E. R., and Ravishankara, A. R.: Bias in filter-based aerosol light absorption measurements due to organic aerosol loading: evidence from ambient measurements, *Aerosol Sci. Tech.*, 42, 1033–1041, 2008.

Lack, D. A., Richardson, M. S., Law, D., Langridge, J. M., Cappa, C. D., McLaughlin, R. J., and Murphy, D. M.: Aircraft instrument for comprehensive characterization of aerosol optical properties, part 2: black and brown carbon absorption and absorption enhancement measured with photo acoustic spectroscopy, *Aerosol Sci. Tech.*, 46, 555–568, 2012.

Lack, D. A., Moosmüller, H., McMeeking, G. R., Chakrabarty, R. K., and Baumgardner, D.: Characterizing elemental, equivalent black, and refractory black carbon aerosol particles: a review of techniques, their limitations and uncertainties, *Anal. Bioanal. Chem.*, 406, 99–122, 2014.

Langridge, J. M., Richardson, M. S., Lack, D., Law, D., and Murphy, D. M.: Aircraft instrument for comprehensive characterization of aerosol optical properties, part I: wavelength-dependent optical extinction and its relative humidity dependence measured using cavity ringdown spectroscopy, *Aerosol Sci. Tech.*, 45, 1305–1318, 2011.

Langridge, J. M., Richardson, M. S., Lack, D. L., Brock, C. A., and Murphy, D. M.: Limitations of the photoacoustic technique for aerosol absorption measurement at high relative humidity, *Aerosol Sci. Tech.*, 47, 1163–1173, 2013.

Lang-Yona, N., Rudich, Y., Segre, E., Dinar, E., and Abo-Riziq, A.: Complex refractive indices of aerosols retrieved by continuous wave-cavity ring down aerosol spectrometer, *Anal. Chem.*, 81, 1762–1769, 2009.

Laven, P.: MiePlot, available at: <http://www.philiplaven.com/MiePlot.htm> (last access: 2 July 2013), 2006.

Lewis, K., Arnott, W. P., Moosmüller, H., and Wold, C. E.: Strong spectral variation of biomass smoke light absorption and single scattering albedo observed with a novel dual wavelength

Development of a cavity enhanced aerosol albedometer

W. Zhao et al.

Title Page

Abstract

Introduction

Conclusions

References

Tables

Figures

◀

▶

◀

▶

Back

Close

Full Screen / Esc

Printer-friendly Version

Interactive Discussion

photoacoustic instrument, *J. Geophys. Res.*, 113, D16203, doi:10.1029/2007JD009699, 2008.

Li, L., Chen, J. M., Chen, H., Yang, X., Tang, Y., and Zhang, R.: Monitoring optical properties of aerosols with cavity ring-down spectroscopy, *J. Aerosol Sci.*, 42, 277–284, 2011.

Ma, L. and Thompson, J. E.: Optical properties of dispersed aerosols in the near ultraviolet (355 nm): measurement approach and initial data, *Anal. Chem.*, 84, 5611–5617, 2012.

Ma, L., Cao, T., and Thompson, J. E.: Technical Note: Aeolian dust proxies produce visible luminescence upon intense laser-illumination that results from incandescence of internally mixed carbon, *Atmos. Meas. Tech. Discuss.*, 6, 5173–5194, doi:10.5194/amtd-6-5173-2013, 2013.

Massoli, P., Murphy, D. M., Lack, D. A., Baynard, T., Brock, C. A., and Lovejoy, E. R.: Uncertainty in light scattering measurements by TSI nephelometer: results from laboratory studies and implications for ambient measurements, *Aerosol Sci. Tech.*, 43, 1064–1074, 2009.

Massoli, P., Kebedian, P. L., Onasch, T. B., Hills, F. B., and Freedman, A.: Aerosol light extinction measurements by Cavity Attenuated Phase Shift (CAPS) spectroscopy: laboratory validation and field deployment of a compact aerosol particle extinction monitor, *Aerosol Sci. Tech.*, 44, 428–435, 2010.

Mellon, D., King, S. J., Kim, J., Reid, J. P., and Orr-Ewing, A. J.: Measurements of extinction by aerosol particles in the near-infrared using continuous wave cavity ring-down spectroscopy, *J. Phys. Chem. A*, 115, 774–783, 2011.

Michel Flores, J., Bar-Or, R. Z., Bluvshstein, N., Abo-Riziq, A., Kostinski, A., Borrmann, S., Koren, I., Koren, I., and Rudich, Y.: Absorbing aerosols at high relative humidity: linking hygroscopic growth to optical properties, *Atmos. Chem. Phys.*, 12, 5511–5521, doi:10.5194/acp-12-5511-2012, 2012.

Moosmüller, H. and Arnott, W. P.: Angular truncation errors in integrating nephelometry, *Rev. Sci. Instrum.*, 74, 3492–3501, 2003.

Moosmüller, H., Varma, R., and Arnott, W. P.: Cavity ring-down and cavity-enhanced detection techniques for the measurement of aerosol extinction, *Aerosol Sci. Tech.*, 39, 30–39, 2005.

Moosmüller, H., Chakrabarty, R. K., and Arnott, W. P.: Aerosol light absorption and its measurement: a review, *J. Quant. Spectrosc. Ra.*, 110, 844–878, 2009.

Müller, T., Nowak, A., Wiedensohler, A., Sheridan, P., Laborde, M., Covert, D. S., Marinoni, A., Imre, K., Henzing, B., Roger, J. C., dos Santos, S. M., Wilhelm, R., Wang, Y. Q., and de

Development of a cavity enhanced aerosol albedometer

W. Zhao et al.

Title Page

Abstract

Introduction

Conclusions

References

Tables

Figures

◀

▶

◀

▶

Back

Close

Full Screen / Esc

Printer-friendly Version

Interactive Discussion



- Leeuw, G.: Angular illumination and truncation of three different integrating nephelometers: implications for empirical, size-based corrections, *Aerosol Sci. Tech.*, 43, 581–586, 2009.
- Naus, H. and Ubachs, W.: Experimental verification of Rayleigh scattering cross sections, *Opt. Lett.*, 25, 347–349, 2000.
- 5 Nikolov, I. D. and Ivanov, C. D.: Optical plastic refractive measurements in the visible and the near-infrared regions, *Appl. Optics*, 39, 2067–2070, 2000.
- Pettersson, A., Lovejoy, E. R., Brock, C. A., Brown, S. S., and Ravishankara, A. R.: Measurement of aerosol optical extinction at 532 nm with pulsed cavity ring down spectroscopy, *J. Aerosol Sci.*, 35, 995–1011, 2004.
- 10 Petzold, A., Onasch, T., Kebabian, P., and Freedman, A.: Intercomparison of a Cavity Attenuated Phase Shift-based extinction monitor (CAPS PMex) with an integrating nephelometer and a filter-based absorption monitor, *Atmos. Meas. Tech.*, 6, 1141–1151, doi:10.5194/amt-6-1141-2013, 2013.
- Ramanathan, V., Crutzen, P. J., Kiehl, J. T., and Rosenfeld, D.: Aerosols, climate, and the hydrological cycle, *Science*, 294, 2119–2124, 2001.
- 15 Rothman, L. S., Gordon, I. E., Barbe, A., Benner, D. C., Bernath, P. F., Birk, M., Boudon, V., Brown, L. R., Campargue, A., Champion, J.-P., Chance, K., Coudert, L. H., Dana, V., Devi, V. M., Fally, S., Flaud, J.-M., Gamache, R. R., Goldman, A., Jacquemart, D., Kleiner, I., Lacombe, N., Lafferty, W. J., Mandin, J.-Y.; Massie, S. T., Mikhailenko, S. N., Miller, C. E., Moazzen-Ahmadi, N., Naumenko, O. V., Nikitin, A. V., Orphal, J., Perevalov, V. I., Perrin, A., Predoi-Cross, A., Rinsland, C. P., Rotger, M., Šimečková, M., Smith, M. A. H., Sung, K., Tashkun, S. A., Tennyson, J., Toth, R. A., Vandaele, A. C., and Vander Auwera, J.: The HITRAN 2008 molecular spectroscopic database, *J. Quant. Spectrosc. Ra.*, 110, 533–572, 2009.
- 20 Sanford, T. J., Murphy, D. M., Thomson, D. S., and Fox, R. W.: Albedo measurements and optical sizing of single aerosol particles, *Aerosol Sci. Tech.*, 42, 958–969, 2008.
- Saphey, A. D., Hill, E. S., Settersten, T., and Linne, M. A.: Fixed-frequency cavity ring down diagnostic for atmospheric particulate matter, *Opt. Lett.*, 23, 954–956, 1998.
- 25 Schnaiter, M., Horvath, H., Möhler, O., Naumann, K. H., Saathoff, H., and Schöck, O. W.: UV-VIS-NIR spectral optical properties of soot and soot-containing aerosols, *J. Aerosol Sci.*, 34, 1421–1444, 2003.
- 30

Development of a cavity enhanced aerosol albedometer

W. Zhao et al.

Title Page

Abstract

Introduction

Conclusions

References

Tables

Figures

◀

▶

◀

▶

Back

Close

Full Screen / Esc

Printer-friendly Version

Interactive Discussion

Shardanand, S. and Rao, A. D. P.: Absolute Rayleigh scattering cross sections of gases and freons of stratospheric interest in the visible and ultraviolet regions, NASA Technical Note, 1977.

Sharma, N., Arnold, I. J., Moosmüller, H., Arnott, W. P., and Mazzoleni, C.: Photoacoustic and nephelometric spectroscopy of aerosol optical properties with a supercontinuum light source, *Atmos. Meas. Tech.*, 6, 3501–3513, doi:10.5194/amt-6-3501-2013, 2013.

Sheridan, P. J., Arnott, W. P., Ogren, J. A., Andrews, E., Atkinson, D. B., Covert, D. S., Moosmüller, H., Petzold, A., Schmid, B., Strawa, A. W., Varma, R., and Virkkula, A.: The Reno Aerosol Optics Study: an evaluation of aerosol absorption measurement methods, *Aerosol Sci. Tech.*, 39, 1–16, 2005.

Slowik, J. G., Cross, E. S., Han, J. H., Davidovits, P., Onasch, T. B., Jayne, J. T., Williams, L. R., Canagaratna, M. R., Worsnop, D. R., Chakrabarty, R. K., Moosmüller, H., Arnott, W. P., Schwarz, J. P., Gao, R. S., Fahey, D. W., Kok, G. L., and Petzold, A.: An inter-comparison of instruments measuring black carbon content of soot particles, *Aerosol Sci. Tech.*, 41, 295–314, 2007.

Smith, J. D. and Atkinson, D. B.: A portable pulsed cavity ring-down transmissometer for measurement of the optical extinction of the atmospheric aerosol, *Analyst*, 126, 1216–1220, 2001.

Sneep, M. and Ubachs, W.: Direct measurement of the Rayleigh scattering cross section in various gases, *J. Quant. Spectrosc. Ra.*, 92, 293–310, 2005.

Strawa, A. W., Castaneda, R., Owano, T., Baer, D. S., and Paldus, B. A.: The measurement of aerosol optical properties using continuous wave cavity ring-down techniques, *J. Atmos. Ocean. Technol.*, 20, 454–465, 2003.

Strawa, A. W., Elleman, R., Hallar, A. G., Covert, D., Ricci, K., Provencal, R., Owano, T. W., Jonsson, H. H., Schmid, B., Luu, A. P., Bokarius, K., and Andrews, E.: Comparison of in situ aerosol extinction and scattering coefficient measurements made during the aerosol intensive operating period, *J. Geophys. Res.*, 111, D05S03, doi:10.1029/2005JD006056, 2006.

Subramanian, R., Roden, C. A., Boparai, P., and Bond, T. C.: Yellow beads and missing particles: trouble ahead for filter-based absorption measurements, *Aerosol Sci. Tech.*, 41, 630–637, 2007.

Thalman, R. and Volkamer, R.: Inherent calibration of a blue LED-CE-DOAS instrument to measure iodine oxide, glyoxal, methyl glyoxal, nitrogen dioxide, water vapour and aerosol

**Development of
a cavity enhanced
aerosol albedometer**

W. Zhao et al.

Title Page

Abstract

Introduction

Conclusions

References

Tables

Figures

◀

▶

◀

▶

Back

Close

Full Screen / Esc

Printer-friendly Version

Interactive Discussion



extinction in open cavity mode, *Atmos. Meas. Tech.*, 3, 1797–1814, doi:10.5194/amt-3-1797-2010, 2010.

Thompson, J. E. and Spangler, H. D.: Tungsten source integrated cavity output spectroscopy for the determination of ambient atmospheric extinction coefficient, *Appl. Optics*, 45, 2465–2473, 2006.

Thompson, J. E., Smith, B. W., and Winefordner, J. D.: Monitoring atmospheric particulate matter through cavity ring-down spectroscopy, *Anal. Chem.*, 74, 1962–1967, 2002.

Thompson, J. E., Barta, N., Policarpio, D., and DuVall, R.: A fixed frequency aerosol albedometer, *Opt. Express*, 16, 2191–2205, 2008.

Vandaele, A. C., Hermans, C., Fally, S., Carleer, M., Colin, R., Mérienne, M. F., Jenouvrier, A., and Coquart, B.: High resolution Fourier transform measurement of the NO₂ visible and near-infrared absorption cross sections: temperature and pressure effects, *J. Geophys. Res.*, 107, 4348, doi:10.1029/2001JD000971, 2002.

Varma, R., Moosmüller, H., and Arnott, W. P.: Toward an ideal integrating nephelometer, *Opt. Lett.*, 28, 1007–1009, 2003.

Varma, R. M., Venables, D. S., Ruth, A. A., Heitmann, U., Schlosser, E., and Dixneuf, S.: Long optical cavities for open-path monitoring of atmospheric trace gases and aerosol extinction, *Appl. Optics*, 48, B159–B171, 2009.

Varma, R. M., Ball, S. M., Brauers, T., Dorn, H.-P., Heitmann, U., Jones, R. L., Platt, U., Pöhler, D., Ruth, A. A., Shillings, A. J. L., Thieser, J., Wahner, A., and Venables, D. S.: Light extinction by secondary organic aerosol: an intercomparison of three broadband cavity spectrometers, *Atmos. Meas. Tech.*, 6, 3115–3130, doi:10.5194/amt-6-3115-2013, 2013.

Villena, G., Bejan, I., Kurtenbach, R., Wiesen, P., and Kleffmann, J.: Interferences of commercial NO₂ instruments in the urban atmosphere and in a smog chamber, *Atmos. Meas. Tech.*, 5, 149–159, doi:10.5194/amt-5-149-2012, 2012.

Virkkula, A., Ahlquist, N., Covert, D., Sheridan, P., Arnott, W., and Ogren, J.: A three-wavelength optical extinction cell for measuring aerosol light extinction and its application to determining light absorption coefficient, *Aerosol Sci. Tech.*, 39, 52–67, 2005.

Wang, L., Wang, W., and Ge, M.: Extinction efficiencies of mixed aerosols measured by aerosol cavity ring down spectrometry, *Chinese Sci. Bull.*, 57, 2567–2573, 2012.

Washenfelder, R. A., Langford, A. O., Fuchs, H., and Brown, S. S.: Measurement of glyoxal using an incoherent broadband cavity enhanced absorption spectrometer, *Atmos. Chem. Phys.*, 8, 7779–7793, doi:10.5194/acp-8-7779-2008, 2008.

**Development of
a cavity enhanced
aerosol albedometer**

W. Zhao et al.

Title Page

Abstract

Introduction

Conclusions

References

Tables

Figures

◀

▶

◀

▶

Back

Close

Full Screen / Esc

Printer-friendly Version

Interactive Discussion



Washenfelder, R. A., Flores, J. M., Brock, C. A., Brown, S. S., and Rudich, Y.: Broadband measurements of aerosol extinction in the ultraviolet spectral region, *Atmos. Meas. Tech.*, 6, 861–877, doi:10.5194/amt-6-861-2013, 2013.

Wei, Y., Ma, L., Cao, T., Zhang, Q., Wu, J., Buseck, P. R., and Thompson, J. E.: Light scattering and extinction measurements combined with laser-induced incandescence for the real-time determination of soot mass absorption cross section, *Anal. Chem.*, 85, 9181–9188, 2013a.

Wei, Y., Zhang, Q., and Thompson, J. E.: Atmospheric black carbon can exhibit enhanced light absorption at high relative humidity, *Atmos. Chem. Phys. Discuss.*, 13, 29413–29445, doi:10.5194/acpd-13-29413-2013, 2013b.

Wilson, E. M., Chen, J., Varma, R. M., Wenger, J. C., and Venables, D. S.: A novel, broadband spectroscopic method to measure the extinction coefficient of aerosols in the near-ultraviolet, *AIP Conf. Proc.*, 1531, 155–158, 2013.

Wu, T., Zhao, W., Chen, W., Zhang, W., and Gao, X.: Incoherent broadband cavity enhanced absorption spectroscopy for in situ measurements of NO₂ with a blue light emitting diode, *Appl. Phys. B*, 94, 85–94, 2009.

Yu, F., Luo, G., and Ma, X.: Regional and global modeling of aerosol optical properties with a size, composition, and mixing state resolved particle microphysics model, *Atmos. Chem. Phys.*, 12, 5719–5736, doi:10.5194/acp-12-5719-2012, 2012.

Zarzana, K. J., De Haan, D. O., Freedman, M. A., Hasenkopf, C. A., and Tolbert, M. A.: Optical Properties of the Products of α -Dicarbonyl and Amine Reactions in Simulated Cloud Droplets, *Environ. Sci. Technol.*, 46, 4845–4851, 2012.

Zhang, R., Khalizov, A. F., Pagels, J., Zhang, D., Xue, H., and McMurry, P. H.: Variability in morphology, hygroscopicity, and optical properties of soot aerosols during atmospheric processing, *P. Natl. Acad. Sci. USA*, 105, 10291–10296, 2008.

Zhao, W., Dong, M., Chen, W., Gu, X., Hu, C., Gao, X., Huang, W., and Zhang, W.: Wavelength-resolved optical extinction measurements of aerosols using broad-band cavity-enhanced absorption spectroscopy over the spectral range of 445–480 nm, *Anal. Chem.*, 85, 2260–2268, 2013.

Development of a cavity enhanced aerosol albedometer

W. Zhao et al.

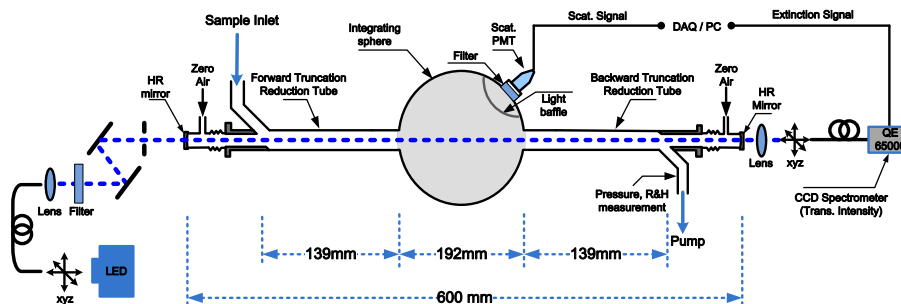


Fig. 1. Schematic diagram of the developed blue LED based cavity enhanced albedometer.

Title Page

Abstract

Introduction

Conclusions

References

Tables

Figures

◀

▶

◀

▶

Back

Close

Full Screen / Esc

Printer-friendly Version

Interactive Discussion



Development of a cavity enhanced aerosol albedometer

W. Zhao et al.

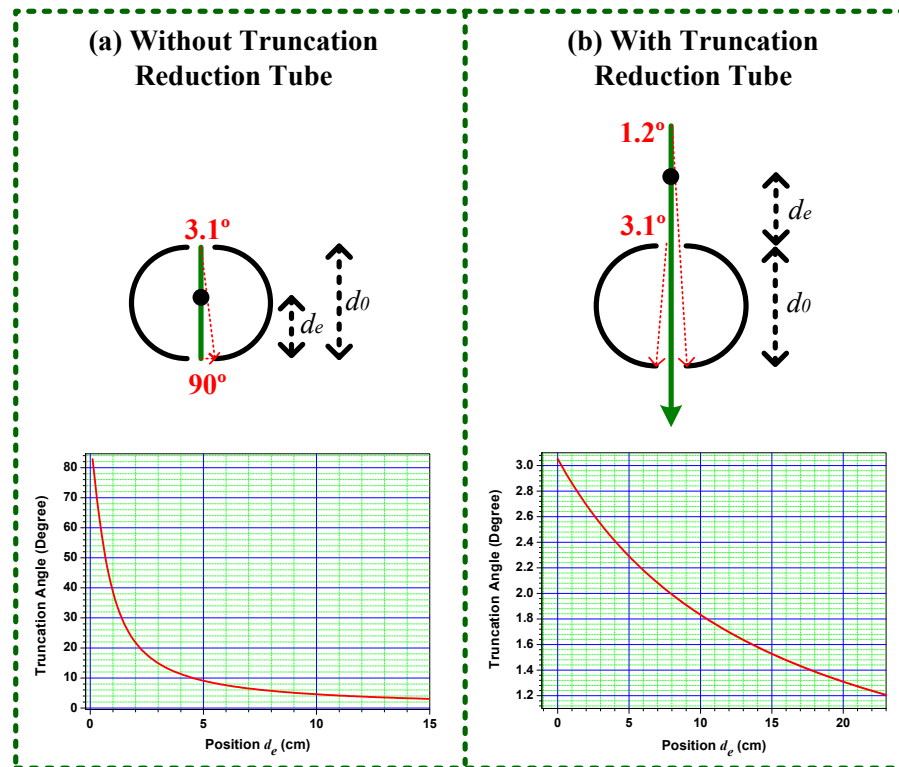


Fig. 2. Forward scattering truncation geometry of cavity enhanced albedometer and plot of truncation angles as a function of the distance d_e from the scattering location in the sphere (marked with a black dot) to the exit or entrance aperture: **(a)** without and **(b)** with truncation reduction tube.

Title Page

Abstract

Introduction

Conclusions

References

Tables

Figures

◀

▶

◀

▶

Back

Close

Full Screen / Esc

Printer-friendly Version

Interactive Discussion



Development of a cavity enhanced aerosol albedometer

W. Zhao et al.

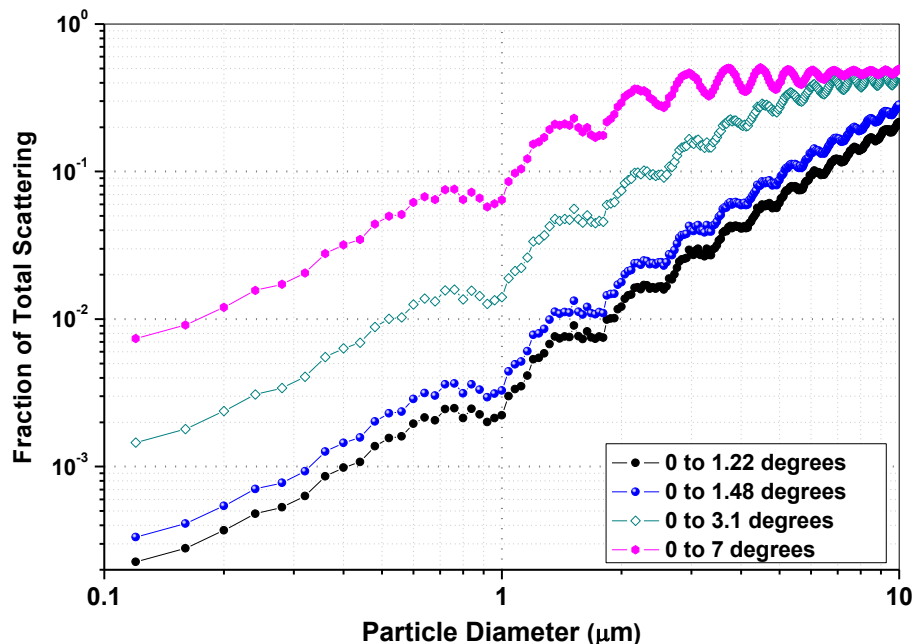


Fig. 3. Size dependence of the truncated fraction of total scattering under different truncation angles: (1) 0–1.22°, calculated with $d_e = (d - d_0)/2$; (2) 0–1.48°: with $d_e = (L - d_0)/2$; (3) 0–3.1°: without truncation reduced tubes; and (4) 0–7°: for the used TSI Nephelometer. The simulations were made based on Mie scattering theory applied to monodisperse particles with a refractive index of $m = 1.6 + i0$ at $\lambda = 470$ nm.

Title Page

Abstract

Introduction

Conclusions

References

Tables

Figures

◀

▶

◀

▶

Back

Close

Full Screen / Esc

Printer-friendly Version

Interactive Discussion



Development of a cavity enhanced aerosol albedometer

W. Zhao et al.

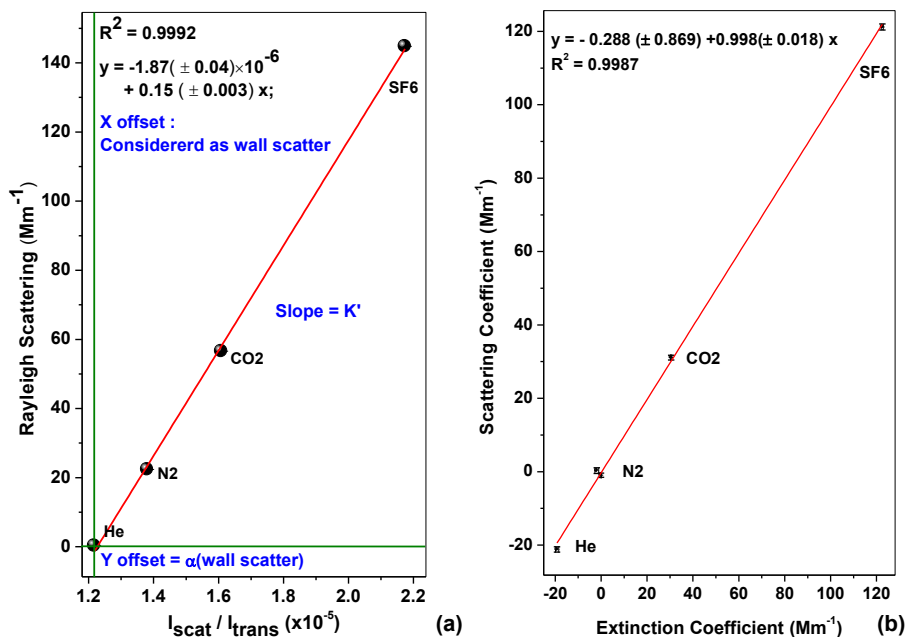


Fig. 4. Calibration of the scaling factor K' of the cavity enhanced albedometer for the scattering channel with He, N₂, CO₂ and SF₆ at $\lambda = 470 \text{ nm}$. **(a)** Plot of $I_{\text{scat}}/I_{\text{trans}}$ vs. theoretical value of the Rayleigh scattering coefficient of each gas. **(b)** Regression plot of the measured extinction and scattering coefficients for calibration.

Title Page

Abstract

Introduction

Conclusions

References

Tables

Figures

◀

▶

◀

▶

Back

Close

Full Screen / Esc

Printer-friendly Version

Interactive Discussion



Development of
a cavity enhanced
aerosol albedometer

W. Zhao et al.

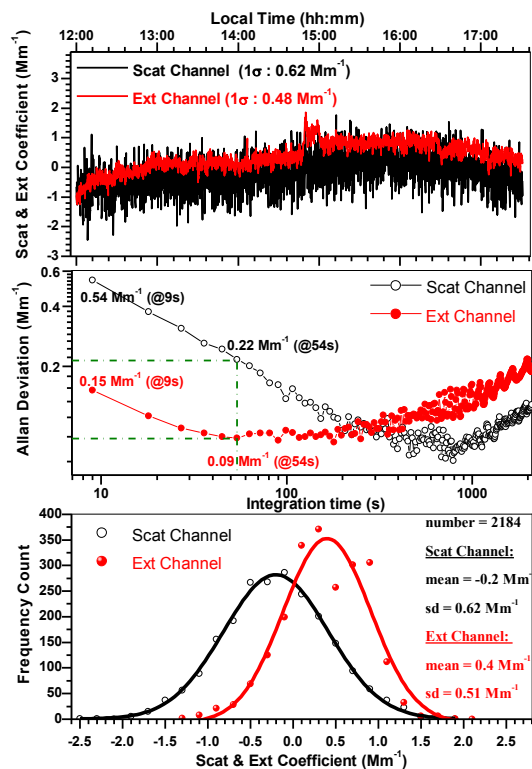


Fig. 5. Time series of a 5.5 h measurement of a particle free zero air sample with a time resolution of 9 s (upper panel) and corresponding Allan variance Plots (middle panel) for both the scattering and extinction channels. The lower panel shows frequency distribution of the performed scattering and extinction measurements. A normal distribution was fitted to the histograms. The 1σ standard deviation, sd , is a measure of the instrument precision; and $mean$ denotes the mean scattering or extinction coefficients.

Development of a cavity enhanced aerosol albedometer

W. Zhao et al.

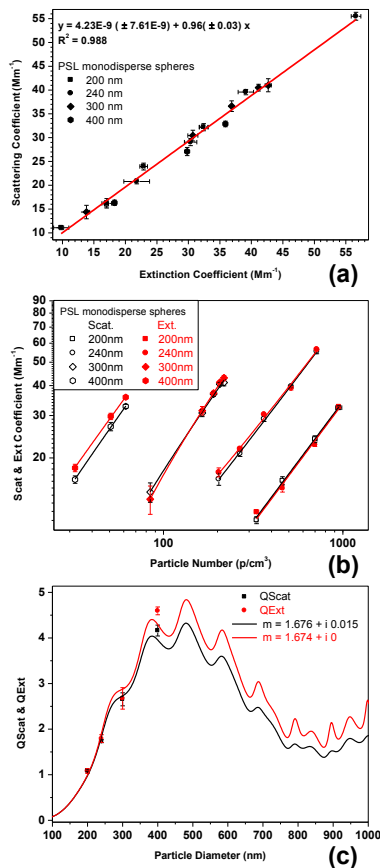


Fig. 6. (a) Regression plot of the measured extinction and scattering coefficients, (b) scattering and extinction coefficients as a function of particle concentration, and (c) the scattering (Q_{Scat}) and extinction (Q_{Ext}) efficiencies as a function of particle diameter for monodisperse PSL spheres with four different particle diameters (200, 240, 300 and 400 nm) at $\lambda = 470$ nm.

Development of
a cavity enhanced
aerosol albedometer

W. Zhao et al.

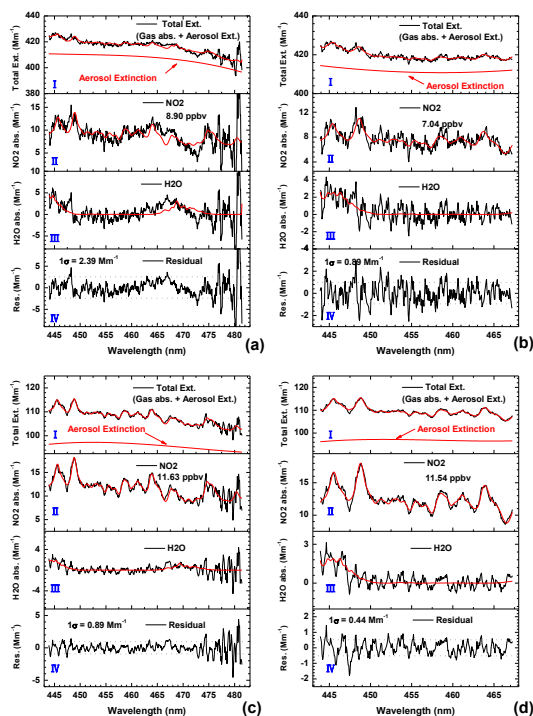


Fig. 7. Example spectra from ambient measurements at different aerosol loadings. **(a), (b)** Aerosol extinction larger than 400 Mm^{-1} ; **(c), (d)** aerosol extinction lower than 100 Mm^{-1} . **(a), (c)** Fit in a window of 444–481 nm for retrieval of aerosol extinction. **(b), (d)** Fit in a window of 444–467 nm for NO_2 concentration retrieval. Black lines: measured spectra; Red lines: aerosol extinction and reference spectra. (I): measured IBBCEAS spectra associated with fitted spectra (including gas absorption and aerosol extinction). (II), (III): fitted NO_2 and H_2O absorption spectra. (IV) fit residuals.

Title Page

Abstract

Introduction

Conclusions

References

Tables

Figures

◀

▶

◀

▶

Back

Close

Full Screen / Esc

Printer-friendly Version

Interactive Discussion



Development of a cavity enhanced aerosol albedometer

W. Zhao et al.

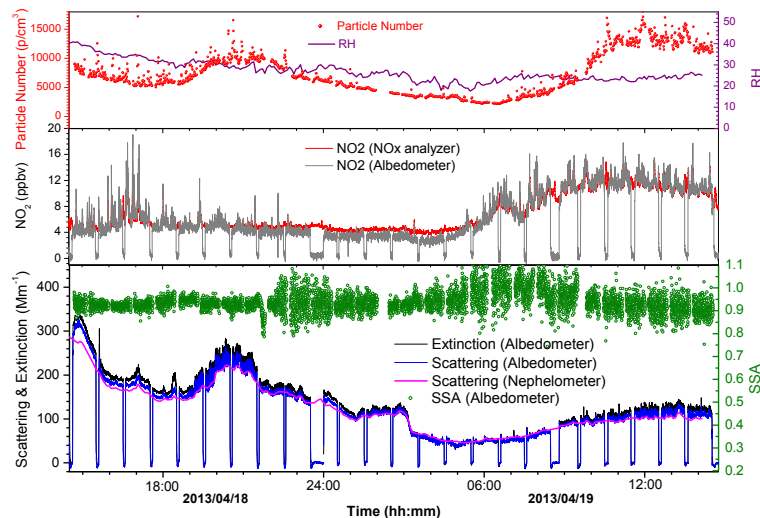


Fig. 8. Ambient air measurements over 24 h using the developed cavity enhanced albedometer. The acquisition time for each data point was 9 s. **(a)** upper panel: relative humidity of the air sample (purple line) measured with a hygromer humidity sensor, and particle concentration (red dot) measured with a CPC at the outlet. **(b)** middle panel: intercomparison of NO_2 concentration measurements (gray line) between the albedometer and a chemiluminescence detector (red line). **(c)** lower panel: aerosol scattering (blue line), extinction (black line) coefficients and the corresponding SSA (olive dot) determined at $\lambda = 470$ nm of the ambient air sample measured with the albedometer. The scattering coefficient was compared with the measurement from a TSI 3563 integrating nephelometer (magenta line). A good agreement between the albedometer and the TSI nephelometer was observed. The scattering coefficients measured with the cavity enhanced albedometer were a little larger than that from the TSI 3563. This difference was properly due to the large truncation angles induced scattering losses in the TSI nephelometer. The smaller truncation angle of our integrating sphere nephelometer allowed for collection of more scattered light.

Development of
a cavity enhanced
aerosol albedometer

W. Zhao et al.

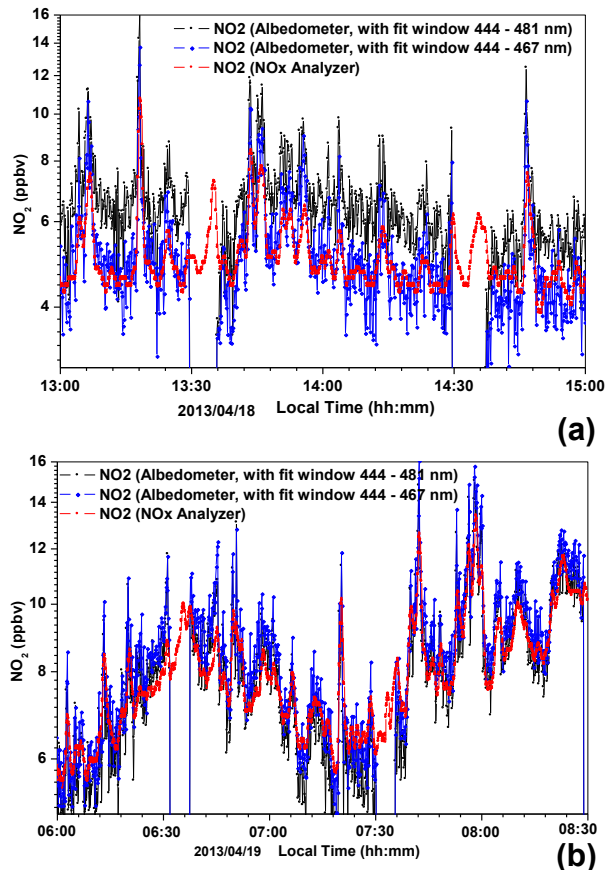


Fig. 9. Comparison of NO₂ concentration measurements in representative time intervals between a NO_x analyzer (red dot line) and the cavity enhanced albedometer using different fit window (black: fitted over 444–481 nm, blue: fitted over 444–467 nm). **(a)** High aerosol extinction condition and **(b)** low aerosol extinction condition.

**Development of
a cavity enhanced
aerosol albedometer**

W. Zhao et al.

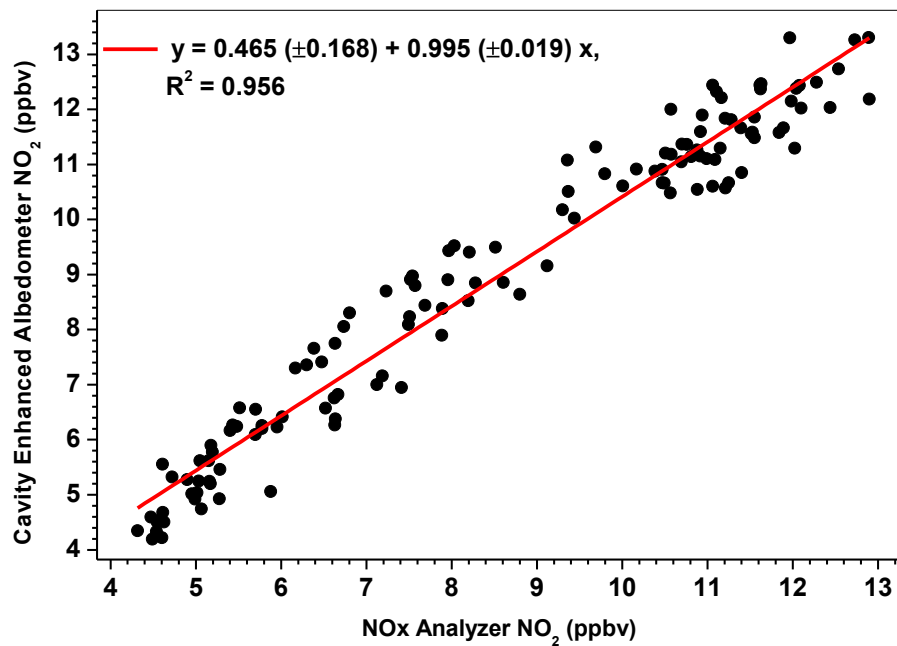


Fig. 10. Correlation plots between NO₂ mixing ratios measured with the cavity enhanced albedometer and a NO_x analyzer. Each data was five minutes averaged.

Title Page

Abstract

Introduction

Conclusions

References

Tables

Figures

◀

▶

◀

▶

Back

Close

Full Screen / Esc

Printer-friendly Version

Interactive Discussion



Development of
a cavity enhanced
aerosol albedometer

W. Zhao et al.

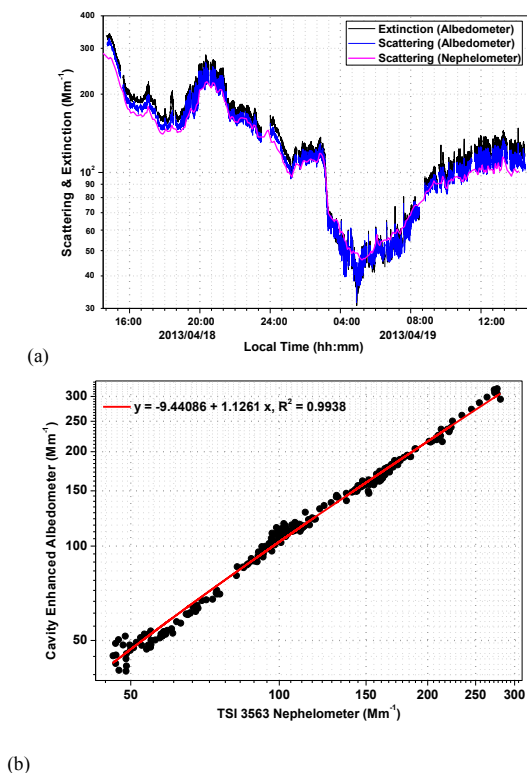


Fig. 11. (a) Enlarged drawing of the scattering and extinction measurements of an air sample. The blue and black lines are the cavity enhanced albedometer measured scattering and extinction coefficients. Magenta line is the scattering coefficient measured with a TSI integrating nephelometer. **(b)** Correlation plots of the scattering coefficients measured by the albedometer and a TSI 3563 nephelometer. Each data was five minutes averaged result.